EPR Investigation of TiO_2 Nanoparticles with Temperature-Dependent Properties

Chinthala Praveen Kumar,[†] Neeruganti Obularajugari Gopal,[‡] Ting Chung Wang,[†] Ming-Show Wong,[‡] and Shyue Chu Ke*,[†]

Physics Department and Materials Science & Engineering Department, National Dong Hwa University, Hualien, Taiwan

Received: December 5, 2005; In Final Form: January 24, 2006

An in situ electron paramagnetic resonance (EPR) study has been carried out for anatase (Hombikat UV100) and rutile TiO_2 nanoparticles at liquid helium (He) temperature (4.2 K) under UV irradiation. Rutile titania was synthesized by ultrasonic irradiation with titanium tetrachloride ($TiCl_4$) as the precursor. XRD and Raman results evidence the crystallinity of titania phases. The nature of trapped electrons and holes has been investigated by EPR spectroscopy under air and vacuum conditions. Illumination of TiO_2 powder (anatase and rutile) at 4.2 K resulted in the detection of electrons being trapped at Ti^{4+} sites within the bulk and holes trapped at lattice oxide ions at the surface. The stability of electron traps was very sensitive to temperature in both phases of TiO_2. The annealing kinetics of the EPR detected radicals has been studied from 4.2 K to ambient temperature and also for calcined titania particles from 523 to 1273 K.

Introduction

Nanostructure materials have received steadily growing interest as a result of their peculiar and fascinating properties, and applications superior to their bulk counterparts.[1,2] Nanocrystalline titania has many important applications such as solar cells,[3] photocatalysts for water photolysis,[4] and degradation of environmental pollutants in air and wastewaters.[5] Titanium dioxide (TiO_2) is a polymorphic substance that is present in three crystalline phases: anatase, rutile, and brookite with different properties and structure. The anatase phase of TiO_2 is generally the higher activity oxidative photocatalyst.[6,7] Comparatively, rutile received less attention in producing photocatalysts.[8] This is attributed to the expectation that the rutile phase may exhibit lower electrochemical performance than the anatase phase, primarily due to differences in their electronic structure.[9] However, rutile has been shown to be effective at both oxidative and reductive chemistry in specific applications.[10] TiO_2 is usually utilized in the forms of both powder and coating. With the decrease in particle size, the photocatalytic performance of TiO_2 is likely to be improved because of smaller particles having larger specific surface. Consequently, the nanosized powder is more effective.[11,12]

Photoexcitation of TiO_2 with its band gap energy (3.2 eV) generates electron−hole (e^-/h^+) pairs, which are trapped at the surface and that can be exploited in various processes at the particle interface. The separation of the electron−hole pairs and their transfer to chemical substrates at the TiO_2 surface is very important for the initiation of photo catalytic reaction and enhancement in reaction rate. In the process of photocatalysis, the electrons and holes produced on photoirradiated TiO_2 powders are trapped at the particle surface to form unpaired electron species. Photocatalytic reactions are actually the reactions of these radicals with reactant molecules at the TiO_2 surface. The EPR characteristics of the photogenerated paramagnetic intermediates have been reported elsewhere.[13−15]

It was suggested that the electron transfer in TiO_2 colloids occurs via surface Ti(IV) atoms which are coordinated with solvent molecules.[16] Meanwhile, the hole transfer occurs via surface oxygen atoms covalently linked to the surface titanium. The photogenerated electrons may be trapped at several sites: on the titanium atoms at the surface or inside the particles, or on oxygen molecules adsorbed on the surface. The photogenerated holes were reported to be trapped at the oxygen atoms in the crystalline lattice near the particle surface or at hydroxyl groups on the surface.[10] EPR spectroscopy has been widely used to examine paramagnetic species on TiO_2 surfaces particularly with the objective of identifying radicals formed under UV irradiation which are important in photocatalytic processes.[13−15] Howe and Gratzel[13] observed EPR spectra of electrons trapped on Ti^{4+} ions and characterized the nature of the Ti^{3+} center on TiO_2. The observations concerning the EPR spectrum of the photogenerated hole adduct species are less clear and EPR signals with different characteristics have been reported.[11,13−15]

Anpo et al.[15] observed EPR spectra of trapped holes following illumination of TiO_2 particles and assigned the signals to $OH^•$ radicals. On the other hand, Howe and Gratzel,[14] in a similar experiment, observed similar EPR spectra and assigned the hole trap to a subsurface oxygen anion radical ($Ti^{4+}O^{•-}Ti^{4+}OH^-$). Recently, Berger et al.[17] have reported the nature of surface photogenerated electrons and holes upon UV irradiation on powdered anatase TiO_2 under vacuum at various temperatures. In their study, the TiO_2 was prepared by the Metal Organic Chemical Vapor Deposition (MOCVD) method and they have concluded that the trapped holes were detected as O^- species, generated from lattice O^{2-} in the valence band. The electrons are detected either as Ti^{3+} species or as electrons captured in the conduction band.

Understanding the reaction pathways available to holes and electrons produced by band gap irradiation of TiO_2 and related materials is essential for various photocatalytic reactions. Though there are many reports about EPR after UV illumina-

* Address correspondence to this author. Phone: +886-3-863-3705. Fax: +886-3-863-2303. E-mail: ke@mail.ndhu.edu.tw.
† Physics Department.
‡ Materials Science & Engineering Department.

10.1021/jp057053t CCC: $33.50
Published on Web 02/22/2006

tion,[13−21] the observations concerning the detection of trapped electrons and holes on TiO_2 nanopowders at lower temperature (4.2 K) illumination conditions are scarce and the majority of such EPR studies until now have been employed for colloidal TiO_2 in different phases. To investigate the nature of electron and hole pairs followed by irradiation of TiO_2, we have studied the EPR spectra at 4 K for photogenerated species formed on anatase and rutile phases of TiO_2 nanopowders. In this paper we also describe the stability, recombination of trapped electrons, and holes from 4.2 K to ambient temperature by EPR investigation.

Experimental Section

The anatase TiO_2 powder (Hombikat UV 100) was obtained from Sachtleben Chemie GmbH as a generous gift. This powder is one of the commercially available TiO_2 powders of 100% anatase. Nanocrystalline rutile TiO_2 was prepared by hydrolysis of $TiCl_4$ as previously described.[22] In a typical synthesis, 110 mL of deionized water was sonicated by employing a direct immersion of titanium horn (MISONIX Sonicator, 3000) for 10 min. At this stage, 10 mL of the precursor ($TiCl_4$) was added to the above water solution which was further sonicated continuously for 2 h. The sonication was conducted without cooling so that a temperature of 353 K was reached at the end of the reaction. The above precipitate containing solution was allowed to stand for 3 h and then separated by centrifugation and washed twice with deionized water. The product was further dried for 18 h at 383 K. The anatase and rutile titania powders were also calcined at different temperatures from 523 to 1273 K for 5 h in air. For EPR measurements in a vacuum, the TiO_2 powder was placed in a sample tube, and then it was evacuated to $\sim 1 \times 10^{-3}$ Torr and sealed off.

Characterization. The crystallinity and particle size of anatase and rutile TiO_2 nanoparticles were investigated by a Rigaku X-ray diffractometer (XRD) operating with Cu Kα radiation at 40 kV and 100 mA. A Dilor Modular XY800 triple-grating Raman spectrometer equipped with a charge-coupled detector (CCD) and a CW Ar-ion laser at 514 nm as the excitation source was used to measure the titania powder structure. BET surface area measurements were determined by the multipoint method on Autosorb 1 (Qunatachrome Instruments Corporation) by N_2 adsorption at 77 K. The UV−vis analysis was performed on a Shimatzu UV-2550 UV−vis spectrophotometer with an integrating sphere reflectance accessory.

The X-band EPR spectra were recorded in situ on a CW Bruker EMX spectrometer equipped with a Bruker TE102 cavity and Advanced Research System Helitran temperature control unit (4−300 K). Samples were cooled to 4.2 K and illuminated within the cavity at that temperature. The samples were irradiated for 60 min directly in the cavity of the EPR spectrometer by a 300-W xenon lamp at a power density of 3 mW/cm^2. The radiation with wavelength ~367 nm was selected by a Pyrex filter. The microwave frequency of ~9.51GHz was used and measured with a Hewlett-Packard 5246L electronic counter. The *g* factor was calibrated by the reference to a DPPH sample (1,1-diphenyl-2-picrylhydrazyl, $g = 2.0037 \pm 0.0002$), but only the first four significant digits are reported. In cases of unresolved rhombic EPR signals, the *g*-values were determined by using the Bruker WINEPR SimFonia simulation package. The high-frequency modulation (100 kHz) was performed by using two Helmholtz coils mounted into the left and right side walls of the cavity. Typical settings for the series of EPR experiments were as follows: center field 3420 G; sweep width 500 G; microwave power 3 mW.

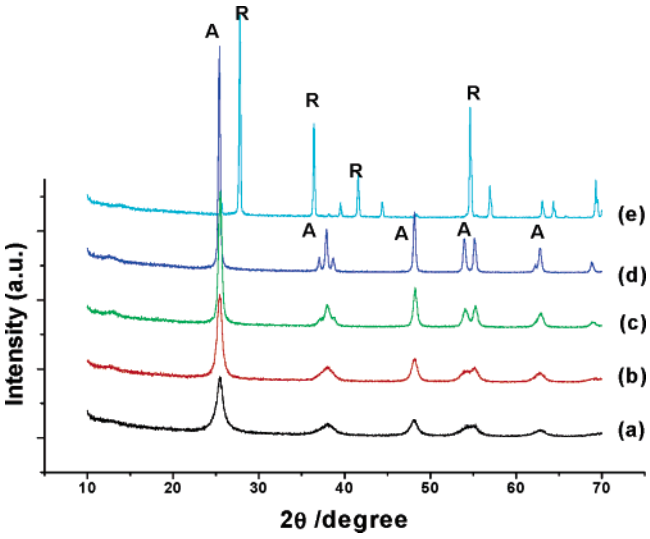

Figure 1. XRD spectra of anatase TiO_2 nanoparticles calcined at various temperatures: (a) 383, (b) 523, (c) 773, (d) 1023, and (e) 1273 K.

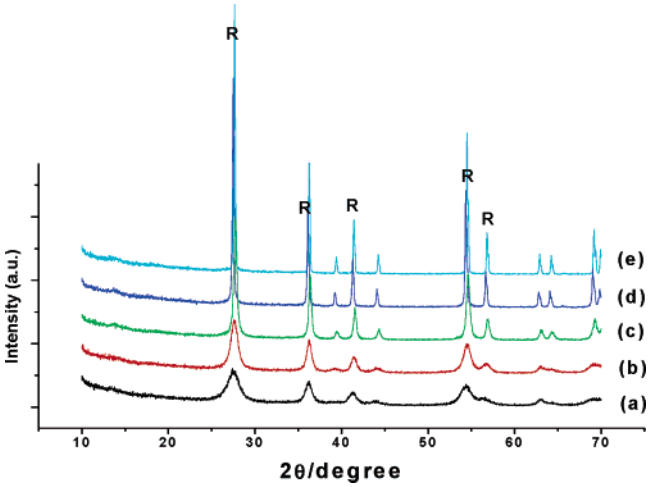

Figure 2. XRD spectra of rutile TiO_2 nanoparticles at various temperatures: (a) 383, (b) 523, (c) 773, (d) 1023, and (e) 1273 K.

Results and Discussion

The XRD and Raman spectra were utilized to analyze the structures of anatase and rutile TiO_2 powders. Figures 1 and 2 show the XRD patterns of anatase and rutile TiO_2 nanopowders calcined in a sequential way to 523, 773, 1023, and 1273 K in a static air atmosphere with a heating rate of 10 deg/min for 5 h. The XRD peaks corresponding to anatase TiO_2 are observed at $2\theta = 25.4°$, 38.4°, 48.1°, and 55° and the peaks at $2\theta = 27.4°$, 36.2°, 41.2°, and 54.5° are due to rutile TiO_2 as shown in Figures 1 and 2, respectively. The BET specific surface area and crystallite sizes of the various TiO_2 particles are as shown in Table 1. The Scherrer equation was applied to measure the crystallite size. The average crystallite size and intensity of peaks increases with increase in calcination temperature of titania. The surface area decreases inversely with increasing calcination temperature from 523 to 1273 K.

Raman spectra show a consistent result of the XRD patterns that the TiO_2 has well-crystallized anatase and rutile structures and are shown in Figures 3 and 4 correspondingly. The anatase titania is characterized by the apparent peaks (Figure 3) at 394,

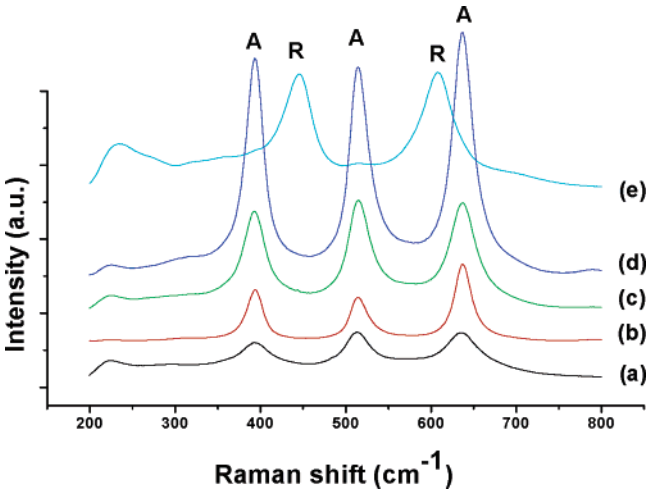

Figure 3. Raman spectra of anatase TiO_2 nanoparticles at various temperatures: (a) 383, (b) 523, (c) 773, (d) 1023, and (e) 1273 K.

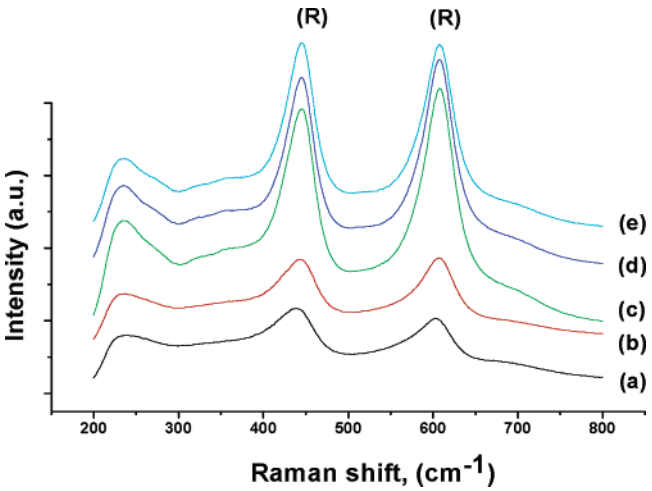

Figure 4. Raman spectra of rutile TiO_2 nanoparticles at various temperatures: (a) 383, (b) 523, (c) 773, (d) 1023, and (e) 1273 K.

TABLE 1: BET Specific Surface Areas and Crystallite Sizes of Various Titania Particles Calcined at Different Temperatures

catalyst	calcination temp (K)	XRD crystal phase	crystal size (nm)	BET surface area (m^2/g)
anatase-TiO_2	383	anatase	12.2	307
anatase-TiO_2	523	anatase	14.1	140
anatase-TiO_2	773	anatase	18.8	68
anatase-TiO_2	1023	anatase	34.9	19
anatase-TiO_2	1273	rutile	68.8	07
rutile	383	rutile	9.5	103
rutile	523	rutile	12.1	52
rutile	773	rutile	21.0	14
rutile	1023	rutile	47.6	7.0
rutile	1273	rutile	71.8	02

513, and 636 cm^{-1},[23] and rutile titania (Figure 4) at 438 and 603 cm^{-1}.[24] The additional band around 230 cm^{-1} is due to an artifact caused by the filter used to remove the Rayleigh scattering. The increase in the intensity of XRD and Raman peaks of titania particles shows the increase in crystallite size. The crystal structure of anatase remains the same until the calcination temperature 1023 K. The TiO_2 phase transformation to rutile can be seen at ~1273 K as shown in Figures 1e and 3e. UV−vis absorption spectra (Figure 5) show that the anatase titania absorbs light at 376 nm and the rutile titania absorbs at 396 nm. Rutile has a smaller band gap of 3.0 eV with excitation

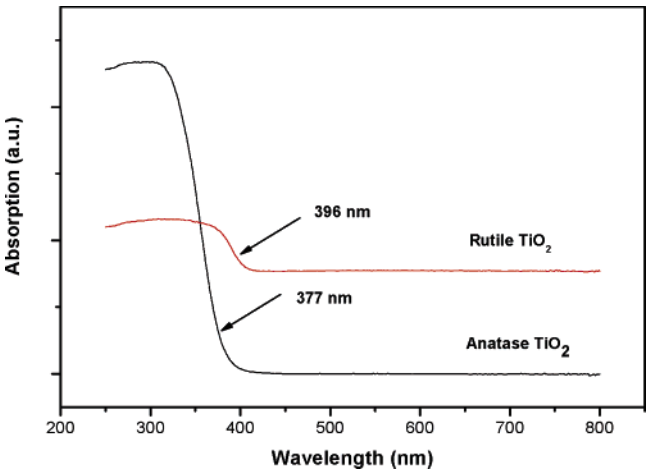

Figure 5. UV−vis spectra of anatase and rutile TiO_2 nanoparticles.

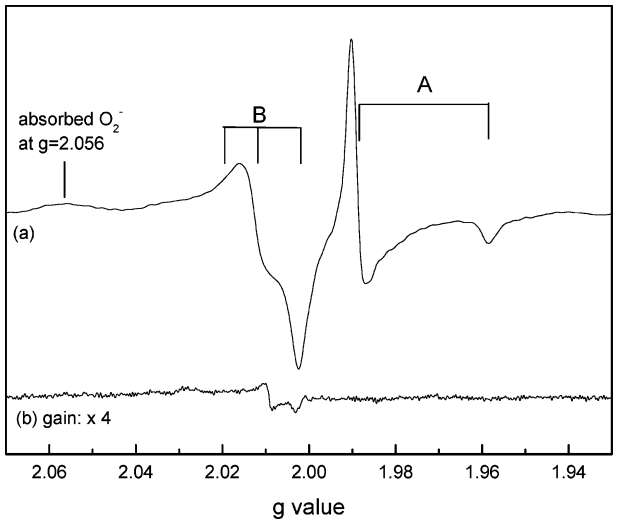

Figure 6. EPR spectra of anatase TiO_2 nanopowder after 1 h of UV illumination at (a) 4.2 and (b) 298 K.

wavelengths, which extends into the near-visible region (~410 nm). Thus, in the present study, the rutile titania synthesized from $TiCl_4$ has absorption at 396 nm.

EPR Signals in Anatase TiO_2. Photoinduced EPR signals of trapped electrons and holes on anatase TiO_2 nanopowder at 4.2 K and at ambient temperature (298 K) in air are shown in Figure 6. In the EPR spectrum at 4.2 K (Figure 6a), there are two sets of features: signals from electrons and holes, which are labeled as signals A and B, respectively. The EPR signals due to anatase TiO_2 are characterized by the sets of g values, $g_1 = 2.016$, $g_2 = 2.012$, $g_3 = 2.002$ and $g_{||} = 1.958$, $g_{\perp} = 1.988$. The sharp signal at $g_{\perp} = 1.988$ and $g_{||} = 1.958$ is assigned to surface electron trapping sites and is represented as signal A.[14,21,25] The EPR signals with g factors $g_1 = 2.016$, $g_2 = 2.012$ and $g_3 = 2.002$ were due to surface hole trapping sites[14,25] and are represented as signal B. When TiO_2 was monitored at ambient temperature during continuous UV illumination, only a very weak signal was observed (Figure 6b) presumably due to hole traps since this signal was found to disappear when UV light stops. These results thus indicate that the lifetime of electron and hole radicals is too short to be observed by EPR at ambient temperature. The system tends to be more ordered as the temperature is reduced to 4.2 K and in view of this the stabilities of electron and hole signals are facilitated by UV illumination at 4.2 K.

TABLE 2: EPR Parameters of Ti^{3+} (electron center) Radicals in Anatase and Rutile TiO_2 Powder along with Literature Values Measured for Similar Species

system/assignment	$g_\perp$	$g_\parallel$	ref
Ti^{3+} (hydrated anatase)	1.990	1.960	14
surface Ti^{3+} in colloidal TiO_2	1.925	1.885	13
Ti^{3+} in solid anatase doped with Sb or Nb	1.990	1.959	39
surface Ti^{3+} in solid anatase TiO_2 in the presence of air and vacuum (Signal A)	1.988	1.958	*a*
inner Ti^{3+} in anatase TiO_2 calcined at 1023 K (Signal C)	1.991	1.962	*a*
Ti^{3+} in Degussa P25 due to rutile phase	1.975	1.940	21
Ti^{3+} in carbon-doped TiO_2	1.9709	1.19	40
surface Ti^{3+} in rutile TiO_2 (Signal F)	1.969	1.947	*a*
inner Ti^{3+} in rutile TiO_2 calcined at 1023 K (Signal L)	1.970	1.944	*a*
vacancy stabilized Ti^{3+} in rutile lattice sites (Signal H)	1.91		*a*

[a] Present work.

TABLE 3: EPR Parameters of Oxygen Related Signals (hole center) in Anatase and Rutile TiO_2 along with Literature Values Measured for Similar Species

	g-tensors			
system/assignment	g_1	g_2	g_3	ref
colloidal anatase TiO_2	2.024	2.014	2.007	37
hydrated TiO_2 anatase particles	2.016	2.012	2.002	14
$^{\bullet}OH$ (on TiO_2 surface)	2.0146	2.0146	2.0032	15
anatase TiO_2 solid in a vacuum	2.018	2.014	2.004	27
anatase TiO_2 solid ($Ti^{4+}O^{\bullet-}Ti^{4+}OH^-$) (signal B)	2.016	2.012	2.002	*a*
anatase TiO_2 solid calcined at 1023 K ($Ti^{4+}O^{2-}Ti^{4+}O^{\bullet-}$) (signal D)	2.026	2.015	2.005	*a*
$Ti^{4+}O^{2-}Ti^{4+}O^{\bullet-}$	2.0273	2.0128	2.0073	37
$Ti^{4+} - O_2^-$ on anatase	2.024	2.009	2.003	41
$O^{\bullet-}$ (rutile + Ga)	2.030	2.023	2.007	42
$O^{\bullet-}$ (rutile + Al)	2.026	2.019	2.003	42
rutile TiO_2 solid dispersed in water		2.03	2.03	43
rutile TiO_2 solid ($Ti^{4+}O^{\bullet-}Ti^{4+}OH^-$) (signal G)	2.019	2.014	2.002	*a*
rutile TiO_2 calcined at 1273 K ($Ti^{4+}O^{2-}$ $Ti^{4+}O^{\bullet-}$) (signal M)	2.026	2.017	2.008	*a*

[a] Present work.

The signals associated with trapped electrons are due to Ti^{3+} in the bulk lattice or at the surface. The Ti^{3+} is produced when electron is adsorbed on Ti^{4+}. When titania semiconductors are irradiated at wavelengths <380 nm, it causes electron excitation from the valence band to the conduction band and a vacancy or hole is left in the valence band. Such holes have the effect of a positive charge. This, in turn, generates the formation of "holes" on the surface of semiconductor, which can react with oxygen, water, and hydroxide ion to form hydroxyl radicals.[26] The photoproduced holes are trapped at the lattice oxygen atoms located in the subsurface layer of the hydrated anatase.[14] This radical has the structure of $Ti^{4+}O^{\bullet-}Ti^{4+}OH^-$ and has the set of g-values of $g_1 = 2.018$, $g_2 = 2.014$, and $g_3 = 2.004$.[14] Previous studies have suggested the location of this hole trap to be either surface or subsurface oxygen anion radicals,[14] or $OH^{\bullet}$ radicals.[27,28] Signal B in Figure 6a corresponds to this signal in the g values, shape, and the surfaces of these samples are covered with hydroxyl groups. From this contemplation, we assign signal B as that due to $Ti^{4+}O^{\bullet-}Ti^{4+}OH^-$ radical. Tables 2 and 3 summarize the **g**-tensors of electron traps (Ti^{3+} sites) and hole traps (oxygen radicals) for anatase TiO_2 for the present work in comparison with literature values. On the basis of these observations we specify the following charge-transfer steps in anatase TiO_2.

$$TiO_2 \rightarrow (e^- + h^+)\ TiO_2 \quad \text{(i)}$$

$$Ti^{4+} + e^- \rightarrow Ti^{3+}\ \text{(trapped electron)} \quad \text{(ii)}$$

$$Ti^{4+}O^{2-}Ti^{4+}OH^- + h^+ \rightarrow Ti^{4+}O^{\bullet-}Ti^{4+}OH^-\ \text{(trapped hole)} \quad \text{(iii)}$$

Temperature Effect on Anatase TiO_2. Figure 7 represents the temperature dependence of the EPR spectra for anatase TiO_2. It should be noted that the temperature-dependent overall EPR signal intensity due to Boltzmann distribution has not been taken into account in plotting the spectra. However, relative variation of the EPR intensities between trapped electrons and holes is obvious in the figure. For the EPR intensity at 4.2 K, the signals are larger and intense. Upon warming from 4.2 to 298 K, the relative intensity of lattice electrons (Ti^{3+}) decreases gradually and disappears around 65 K. Immediate re-cooling from 65 to 4.2 K did not resolve the trapped electron signal. The trapped holes signal intensity was also found to decrease with increasing temperature but was still observed up to 150 K with poor intensity indicating that removal of electrons by adsorbed oxygen stabilizes the trapped holes by preventing recombination. The subsequent disappearance of trapped holes on warming to room temperature is associated with recombination of an electron−hole pair since at higher temperature diffusion of trapped charges becomes favorable.[29]

We have also investigated the EPR analysis at 4.2 K for TiO_2 particles calcined at various temperatures and the corresponding EPR spectra are shown in Figure 8. Signal A decreased for the titania heated at 523 K. When the sample was heated at temperatures above 773 K and at 1023 K, a new set of g-values at $g_\perp = 1.991$ and $g_\parallel = 1.962$ represented as signal C appeared (Figure 8d). These g-values are slightly different from that of surface electron traps (hydrated Ti^{3+}) discussed above and are assigned to inner electron traps (Ti^{3+}) of the particle which will not participate in the surface reaction. The origin of this inner electron trap is due to the nonstoichiometric formation of Ti atoms at the grain boundary and increase of the particle size (Table 1) by heat treatment at temperatures above 773 K. These results are in agreement with those of Nakaoka et al.[25] but they could not detect signal A when the titania sample was heated at 473 and 623 K as their experiments were analyzed at 77 K. The Ti^{3+} formed inside the particles acts as a recombination center and reduces the activity of the surface reactions for heat-treated TiO_2 powders. Signal B did not change much with an increase in calcination temperature from 383 to 523 K. However, signal B was broad in the 773 K sample (Figure 8c) and a weak and new signal at $g = 2.048$ represented as signal E appeared. We have no obvious explanation for this new signal. However, one possible cause is the residual water molecule on the particle surface since when samples are calcined at higher temperatures signal E disappeared.

For samples calcined at 1023 K (Figure 8d), a new hole signal represented as signal D appeared at $g_1 = 2.026$, $g_2 = 2.015$, and $g_3 = 2.005$. Earlier reports[25] have also shown similar results ($g_1 = 2.030$, $g_2 = 2.018$, and $g_3 = 2.004$) and evidenced this signal is not related to the surface hydroxyl group as its g-values are different in water vapor. This is due to the fact that in calcined samples the surface hydroxyl groups are removed by heat treatment. To be consistent with the earlier assignment, signal D thus is assigned to the radical $Ti^{4+}O^{2-}Ti^{4+}O^{\bullet-}$. The titania powder phase transition from anatase to rutile can be seen from Figures 1e and 3e, when it was calcined at 1273 K. The EPR spectrum obtained for this sample (Figure 8e) has not

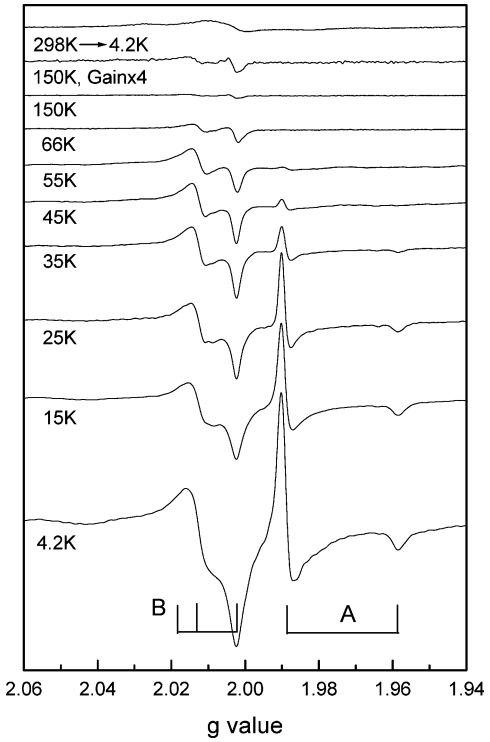

Figure 7. EPR spectrum illustrating the trapped sites in anatase titania powder after 1 h of UV irradiation at 4.2 K in air then monitored at 4.2 K and at different temperatures.

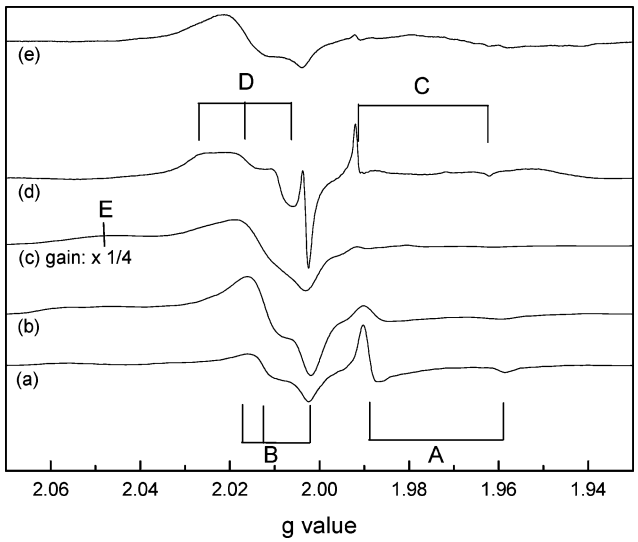

Figure 8. EPR spectra analyzed at 4.2 K for illuminated anatase TiO_2 powder (a) dried at 383 K and (b) calcined at 523, (c) 773, (d) 1023, and (e) 1273 K.

shown any additional signal upon photoirradiation. Nevertheless, there is a weak signal due to hole traps in the range of 2.002 to 2.030.

The EPR results of anatase TiO_2 nanopowder in a vacuum ($\sim 10^{-3}$ Torr) at 4.2 K and at different temperatures are also shown in Figure 9. Irradiation in a vacuum at 4.2 K produced signals due to electrons (Ti^{3+}) and holes the same as the results obtained in air. Analogous to EPR results in air, signal A disappears when it is warmed to 85 K after irradiation at 4.2 K. Immediate recooling from 85 to 4.2 K in vacuum conditions regains the electron trap signal at $g_\perp = 1.989$ with smaller intensity. The disappearance of trapped electrons and holes on warming to higher temperatures is associated with recombination of the electron−hole pair by the formation of O_2^- species, which

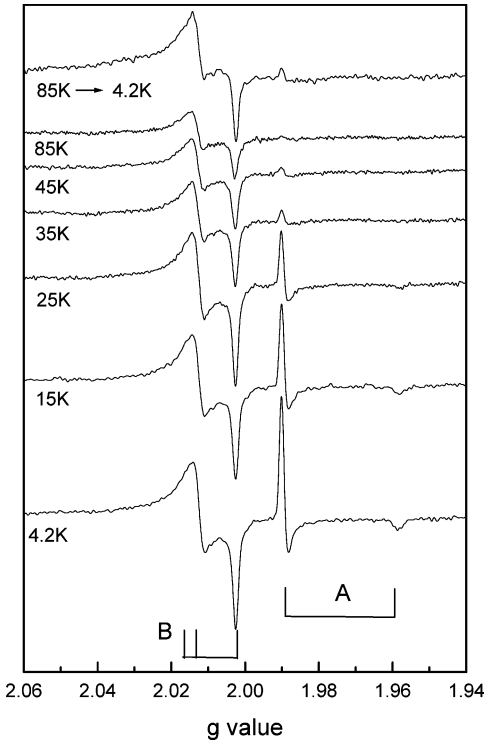

Figure 9. EPR spectrum illustrating the trapped sites in anatase titania powder after 1 h of UV irradiation at 4.2 K in a vacuum then monitored at 4.2 K and at different temperatures.

originate initially from surface hydroxyl groups and trapped holes. Another possible reaction scheme proposed by Gratzel et al.[14] that could also account for the disappearance of trapped electrons and holes is as follows.

$$h^+ + OH^- \rightarrow {}^\bullet OH \quad \text{(iv)}$$

$$2OH^\bullet \rightarrow H_2O_2 \quad \text{(v)}$$

$$H_2O_2 + h^+ \rightarrow O_2^- + 2H^+ \quad \text{(vi)}$$

$$O_2^- + h^+ \rightarrow O_2 \quad \text{(vii)}$$

Upon warming, the reaction of holes with surface hydroxyl groups produces hydroxyl radicals which immediately dimerize to form peroxide and traps another hole to form O_2^-. Subsequent oxidation of absorbed O_2^- by another hole forms absorbed O_2. The spectroscopic evidence for the formation of peroxide during water photolysis was reported by Duonghong et al.[30] Although the formation of oxygen molecules from holes is possible through reactions iv−vii, that implies the trapping of three photogenerated holes without consuming any electrons. This reaction pathway thus contradicts the temperature-dependent results presented in Figure 9, since as evidenced in Figure 9, the majority decrease is trapped electron EPR signals (signal A) rather than the hole signals (signal B). Therefore, it seems to us that the formation of O_2^- by residual adsorbed oxygen molecules is a more plausible explanation for the temperature-dependent data presented here.

EPR Signals and Temperature Effects in Rutile TiO_2. Figure 10 represents the EPR spectra of synthesized rutile TiO_2 recorded at 4.2 K and at ambient temperature with and without UV illumination. For rutile TiO_2 illuminated at 4.2 K (Figure 10a), the light-dependent EPR signals are characterized by two sets of g values, $g_\perp = 1.969$, $g_{||} = 1.947$ (signal F) and $g_1 =$

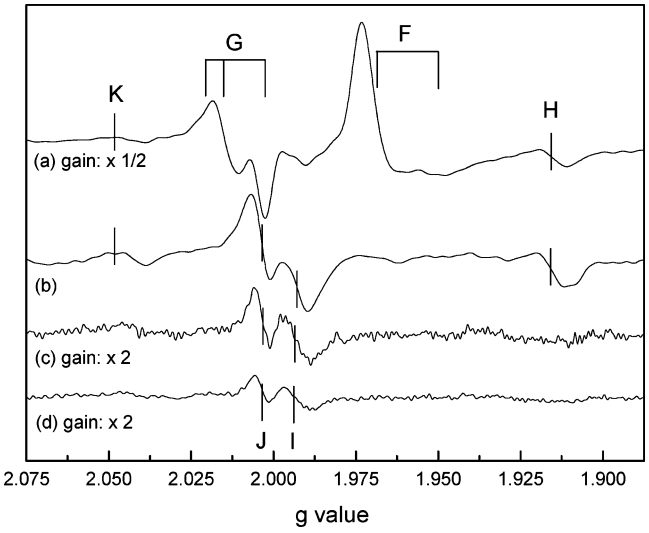

Figure 10. EPR spectra of rutile TiO_2 nanopowder at (a) 4.2 K after 1 h of UV illumination, (b) 4.2 K without UV illumination, (c) 298 K after 1 h of UV illumination, and (d) 298 K without UV illumination.

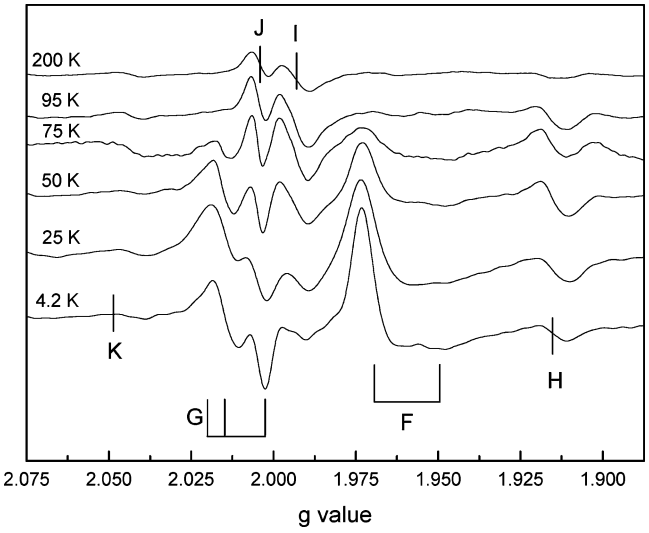

Figure 11. EPR spectrum illustrating the trapped sites in rutile titania powder after 1 h of UV irradiation at 4.2 K then monitored at 4.2 K and at different temperatures.

2.019, $g_2 = 2.014$, $g_3 = 2.002$ (signal G). These signals could not be detected without UV illumination at 4.2 K (Figure 10b) and at ambient temperature (Figure 10d). They also could not be detected when illuminated at ambient temperature (Figure 10c) presumably due to fast recombination effects. Thus, signals F and G are ascribed to the surface electron traps (Ti^{3+})[31,32] and to hole trapping sites, respectively. The hole trapping sites can further be assigned here to the rutile $Ti^{4+}O^{\bullet-}Ti^{4+}OH^-$ radical since its *g*-values coincide well with those observed in anatase TiO_2 (Table 3). The signal H at $g = 1.91$ is assigned to vacancy-stabilized Ti^{3+} in the lattice sites[33,34] based on the comparison of their *g*-values and its formation in the dark. Three additional signals I ($g = 1.994$), J ($g = 2.002$), and K ($g = 2.048$) are also observed which remain as unidentified species. However, these three signals are light independent (Figure 10) and thus are not relevant to the photocatalytic reaction of TiO_2. Most likely, these signals are due to the presence of impurities in the as synthesized rutile sample, for example, signal J could be due to the presence of cationic impurities or electrons trapped in oxygen vacancies.[35,36] Figure 11 shows the temperature dependence of the EPR spectra for rutile TiO_2 powder after UV irradiation at 4.2 K in air. Upon warming, both surface trapped electrons (Ti^{3+}) and hole signals decrease and they were found to be detectable up to 75 K. These results are similar to those described above in anatase titania; we thus propose that the charge-transfer steps (reactions i−iii) are identical in both phases of TiO_2.

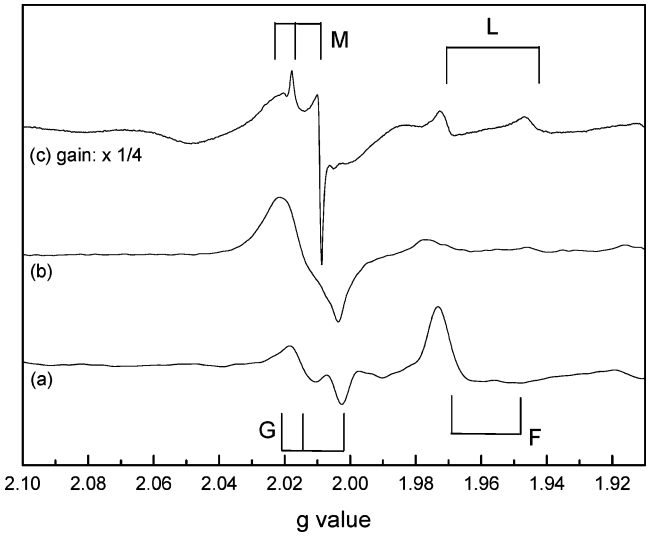

Figure 12. EPR spectra analyzed at 4.2 K for illuminated rutile TiO_2 powder (a) dried at 383 K and (b) calcined at 773 K and (c) 1023 K.

Rutile TiO_2 synthesized from $TiCl_4$ was also calcined at various temperatures to compare the existence of paramagnetic species with the hydrated rutile TiO_2, which was dried at 383 K for 18 h. Figure 12 shows the EPR spectra recorded at 4.2 K for rutile TiO_2 calcined at various temperatures from 773 to 1023 K. In this rutile titania, the signal F due to surface Ti^{3+} disappeared almost completely when the sample was calcined at 773 K and a new signal with $g_\perp = 1.970$ and $g_{||} = 1.944$ represented as signal L appeared when the sample is calcined at 1023 K. Similar to anatase TiO_2 calcined samples, this signal can be assigned to the inner Ti^{3+} of the particle. Signal G (rutile $Ti^{4+}O^{\bullet-}Ti^{4+}OH^-$ radical) observed in as synthesized (Figure 10a) and dried at 383 K (Figure 12a) samples is replaced with a new signal M ($g_1 = 2.026$, $g_2 = 2.017$, and $g_3 = 2.008$) when the sample is calcined at 1023 K (Figure 12c). Micic et al.[37] has reported the radical formation of trapped holes on the surface of TiO_2 colloid ($g_1 = 2.027$, $g_2 = 2.018$, and $g_3 = 2.007$) and assigned it to the $Ti^{4+}O^{2-}$ $Ti^{4+}O^{\bullet-}$ radical. In the present study, the *g*-values of the rutile titania calcined at 1023 K (signal M) are in agreement with the above-reported values provided the surface hydroxyl groups are removed by the heat treatment, thus we assign signal M (Figure 12c) to the rutile $Ti^{4+}O^{2-}$ $Ti^{4+}O^{\bullet-}$ radical. Tables 2 and 3 summarize the **g**-tensors of electron traps (Ti^{3+} sites) and hole traps (oxygen radicals) for rutile TiO_2 in this work. In view of these results, the changes observed upon calcinations mostly are due to the removal of surface hydroxyl and water molecules and the increase of the particle size (Table 1). It has also been reported[38] that the photooxidation activity of TiO_2 nanoparticles decreases with increasing calcination temperature. This may arise from a decrease in the population of surface defect sites with an increase in calcination temperature due to the sintering of TiO_2 particles.

Conclusions

The EPR experiments were used to detect and characterize the electron and hole traps on anatase and rutile TiO_2 nanopowders at 4.2 K. The stability of electron and hole traps on

anatase titana nanoparticles in the presence of air, in a vacuum, and after calcinations has been investigated by EPR spectroscopy. Illumination of anatase and rutile TiO_2 powder at 4.2 K resulted in the formation of trapped electrons (Ti^{3+} centers) and holes (oxygen radicals covalently linked to surface Ti^{4+} atoms). The electron traps generated by UV illumination at 4.2 K in anatase and rutile titania are stable below 85 K and disappeared when they further warmed, whereas the hole traps are more stable up to ~150 K. This is attributed to the adsorption of electrons by oxygen. The further heating to ambient temperature showed the complete disappearance of hole traps due to electron−hole recombination effect. The EPR of calcined titania (anatase and rutile) samples showed that the electron traps signal decreases or disappear with increase in calcinations temperatures up to around 773 K and inner electron traps (Ti^{3+}) appear when they are further calcined above 773 K. Even though anatase TiO_2 is thermodynamically more stable and has greater photocatalytic properties, we have synthesized high purity rutile TiO_2 using $TiCl_4$ and could detect the presence of paramagnetic species by EPR spectroscopy. The method of preparation is simple, cheap, and has very attractive properties as a catalytic support or as a catalyst in photocatalytic applications.

Acknowledgment. The authors are thankful for the financial support of the National Science Council of Taiwan ROC under grant No. NSC-93-2112-M-259-006. The authors gratefully acknowledge the referees for detailed comments and many helpful suggestions.

References and Notes

(1) *Handbook of Nanostructured Materials and Nano Technology*; Nalwa, H. S., Ed.; Academic Press: New York, 2000.
(2) Thiaville, A.; Miltat, J. *Science* **1999**, *284*, 1939.
(3) Tennakone, K.; Jayaweera, P. V. V.; Bandaranayake, P. K. M. *J. Photochem. Photobiol. A* **2003**, *158*, 125.
(4) Matsumoto, Y.; Unal, U.; Tanaka, N.; Kudo, A.; Kato, H. *J. Solid-State Chem.* **2004**, *177*, 4205.
(5) Ollis, D. F.; Al-Ekabi, H. *Proceedings of the 1st International Conference on TiO_2 Photocatalytic Purification and Treatment of Water and Air*, London, Ontario, 1993, Nov. 8−13; Elsevier: Amsterdam, The Netherlands, 1992,
(6) Watababem, T.; Nakajima, A.; Wang, R.; Minabe, M.; Koizumi, S.; Fujishima, A.; Hashimoto, A. *Thin Solid Films* **1999**, *351*, 260.
(7) Sumita, T.; Yamaki, T.; Yamamoto, S.; Miyashita, A. *Appl. Surf. Sci.* **2002**, *200*, 21.
(8) Sun, J.; Gao, L.; Zhang, Q. *J. Am. Ceram. Soc.* **2003**, *86*, 1677.
(9) Hosono, E.; Fujihara, S.; Kakiuchi, K.; Imai, H. *J. Am. Chem. Soc.* **2004**, *126*, 7790.
(10) Park, N.; van de Lagemaat, J.; Frank, A. *J. Phys. Chem. B* **2000**, *104*, 8989.
(11) Anpo, M.; Shima, T.; Kodama, S.; Kubokawa, Y. *J. Phys. Chem.* **1987**, *91*, 4305.
(12) Zhang, Z. B.; Wang, C. C.; Zakaria, R.; Ying, J. Y. *J. Phys. Chem. B* **1998**, *102*, 10871.
(13) Howe, R. F.; Gratzel, M. *J. Phys. Chem.* **1985**, *89*, 4495.
(14) Howe, R. F.; Gratzel, M. *J. Phys. Chem.* **1987**, *91*, 3906.
(15) Anpo, M.; Shima, T.; Kubokawa, Y. *Chem. Lett.* **1985** 1799.
(16) Kolile, U.; Moser, J.; Gratzel, M. *Inorg. Chem.* **1985**, *24*, 2253.
(17) Berger, T.; Sterrer, M.; Diwald, O.; Knozinger, E.; Panayotov, D.; Thomson, T. L.; Yates, J. T., Jr. *J. Phys. Chem. B* **2005**, *109*, 6061.
(18) Riegel, G.; Bolton, J. R. *J. Phys. Chem.* **1995**, *99*, 4215.
(19) Chen, L. X.; Rajh, T.; Wang, Z. Y.; Thurnauer, M. C. *J. Phys. Chem. B* **1997**, *101*, 10688.
(20) Jenkins, C. A.; Murphy, D. M. *J. Phys. Chem. B* **1999**, *103*, 1019.
(21) Hurum, D. C.; Agrios, A. G.; Gray, A.; Rajh, T.; Thurnauer, M. C. *J. Phys. Chem. B* **2003**, *107*, 4545.
(22) Huang, W.; Tang, X.; Wang, Y.; Koltypin, Y.; Gedanken, A. *J. Chem. Soc., Chem. Commun.* **2000**, *15*, 1415.
(23) Kelly, S.; Pollak, F. H.; Tomkiewicz, M. *J. Phys. Chem. B* **1997**, *101*, 2730.
(24) Zhang, F.; Zheng, Z.; Chen, Y.; Liu, D.; Liu, X. *J. Appl. Phys.* **1998**, *83*, 4101.
(25) Nakaoka, Y.; Nosaka, Y. *J. Photochem. Photobiol. A* **1997**, *110*, 299.
(26) Hoffmann, M. R.; Martin, S. T.; Choi, W.; Bahnemann, D. Environmental applications of semiconductor photocatalysis. *Chem. Rev.* **1996**, *95*, 69.
(27) Jaeger, C. D.; Bard, A. J. *J. Am. Chem. Soc.* **1979**, *83*, 3146.
(28) Brezova, V.; Stasko, A.; Lapcik, L., Jr. *J. Photochem. Photobiol. A* **1990**, *59*,115.
(29) Rajh, T.; Ostafin, A. E.; Micic, O. I.; Tiede, D. M.; Thurnauer, M. C. *J. Phys. Chem.* **1996**, *100*, 4538.
(30) Duonghong, D.; Gratzel, M. *J. Chem. Soc., Chem. Commun.* **1984**, 1597.
(31) Li, Y. Z.; Fan, Y. N.; Yang, H. P.; Xu, B. L.; Feng, L. Y.; Yang, M. F.; Chen, Y. *Chem. Phys. Lett.* **2003**, *372*, 160.
(32) Bonneviot, L.; Haller, G. L. *J. Catal.* **1988**, *113*, 96.
(33) Huizinga, T.; Prins, R. *J. Phys. Chem.* **1981**, *85*, 2156.
(34) Fairhurst, S. A.; Inglis, A. D.; Le Page, Y.; Morton, J. R.; Preston, K. F. *Chem. Phys. Lett.* **1983**, *95*, 444.
(35) Henderson, B.; Wertz, J. E. *Adv. Phys.* **1968**, *17*, 749.
(36) Henderson, B.; Hughes, A. E. In *Point defects in solids*; Crawford, J. H., Slifkin, L. M., Eds.; Plenum Press: New York, 1972; p 381
(37) Micic, O. I.; Zhang, Y.; Cromack, K. R.; Trifunac, A. D.; Thurnauer, M. C. *J. Phys. Chem.* **1993**, *97*, 7277.
(38) Sato, S.; Kadowaki, T.; Yamaguti, K. *J. Phys. Chem.* **1984**, *88*, 2930.
(39) Meriaudeau, P.; Che, M.; Jorgensen, C. K. *Chem. Phys. Lett.* **1970**, *5*, 131.
(40) Li, Y.; Hwang, D. S.; Lee, N. H.; Kim, S. J. *Chem. Phys. Lett.* **2005**, *404*, 25.
(41) Coronado, J. M.; Maira, A. J.; Conesa, J. C.; Yeung, K. L.; Augugliaro, V.; Soria, J. *Langmuir* **2001**, *17*, 5368.
(42) Zwingel, D. *Solid State Commun.* **1978**, *26*, 775.
(43) Aundaithai, M.; Kutty, T. R. N. *Mater. Res. Bull.* **1988**, *23*,1675.